N$_2$O decomposition and reduction on Co-MOR, Fe-MOR and Ni-MOR catalysts: *in situ* UV–vis DRS and *operando* FTIR investigation. An insight on the reaction pathways

Daniela Pietrogiacomi[a,b,*], Maria Cristina Campa[b], Lea Roberta Carbone[a], Manlio Occhiuzzi[a,b]

[a] *Dipartimento di Chimica, "Sapienza" Università di Roma, Piazzale Aldo Moro 5, 00185 Roma, Italy*
[b] *CNR-Istituto per lo Studio dei Materiali Nanostrutturati, c/o Dipartimento di Chimica, "Sapienza" Università di Roma, Piazzale Aldo Moro 5, 00185 Roma, Italy*

ARTICLE INFO

ABSTRACT

Co-, Fe- or Ni-exchanged Na-MOR (Si/Al = 9.2) were prepared by ion-exchange method. The catalytic activity for N$_2$O decomposition in the absence or in the presence of NO and for N$_2$O reduction with CH$_4$ in the absence of O$_2$ (CR$_{N_2O}$), or in the presence of O$_2$ (SCR$_{N_2O}$) was investigated. The catalytic measurements were performed in a flow apparatus with GC analysis of reactants and products. On Fe-MOR, *in situ* FTIR and UV–vis characterization evidenced coordinatively unsaturated sites (c.u.s.) Fe^{2+} arising from two families of Fe^{3+} dimers with different reducibility. Characterization and catalytic results combined with *operando* FTIR experiments gave an insight into the transition metal ion (tmi) species working during N$_2$O abatement and into the reaction pathways.

For N$_2$O decomposition the activity order was Co-MOR > Fe-MOR in the absence of NO and Fe-MOR ≥ Co-MOR in the presence of NO, whereas Ni-MOR was always inactive. The decomposition occurred *via* redox mechanism passing through the formation of activated surface oxygen species, O$_{ads}$*. The quasi-oxidic character of this activated oxygen in the Fe^{3+}-O$^{(1+\delta)-}$—Fe$^{(2+\delta)+}$ intermediates with respect to the oxyl character of that in Co^{3+}O$^-$ intermediates accounted for the lower activity and for the activity enhancement by NO addition to the feed of Fe-MOR with respect to Co-MOR. In Ni-MOR, both isolated or dimeric Ni^{2+} species were unable to be oxidized by N$_2$O yielding O$_{ads}$*.

For N$_2$O reduction, (CR$_{N_2O}$) and (SCR$_{N_2O}$), the activity order was Fe-MOR > Ni-MOR > Co-MOR. On all catalysts *operando* FTIR experiments revealed CH$_x$O$_y$ intermediates (methoxy, formaldehyde and two types of formate species). The investigation of surface species changing the addition order of the reactants evidenced that the formation of CH$_x$O$_y$ intermediates was favored on Co-MOR by pre-saturation with N$_2$O, that yielded Co^{3+}O$^-$ able to activate CH$_4$, whereas on Ni-MOR by pre-saturation with CH$_4$, that reduced Ni^{2+} dimers to Ni$^+$ dimers, able to activate N$_2$O. On Fe-MOR, the Fe^{2+} dimers formed during activation behaved as Co^{2+}, whereas the Fe^{2+} dimers formed by reduction with CH$_4$ behaved as Ni$^+$ dimers.

The formation and the stability of O$_{ads}$* surface species were key factors for N$_2$O decomposition and reduction pathways. These factors were affected by the mobility of the tmi electrons, that depends on the oxidation state, nuclearity and location in MOR framework of tmi.

1. Introduction

Nitrous oxide is the third most important anthropogenic greenhouse gas which significantly contributes to the depletion of the stratospheric-ozone layer, having a Global Warming Potential 310 times higher with respect to CO$_2$ and a mean life-time of about 114 years. N$_2$O emissions are rapidly increasing (forecasted to double by 2050) unless mitigation strategies are employed, as committed by the Kyoto Protocol 2005 [1] and by the Paris Agreement 2015 [2]. The concentrated N$_2$O emissions

from fossil fuels combustion and chemical industry can be effectively controlled by end-of-pipe remediation technologies, taking into account the coexistence of other components in off-gases, such as NO$_x$, H$_2$O, and O$_2$. The best available after-treatment technologies for N$_2$O abatement are the direct catalytic decomposition and the Selective Catalytic Reduction (SCR) [3–5]. At present, in the tail-gas of nitric acid plants N$_2$O is abated by decomposition or by SCR with natural gas, while NO$_x$ is abated by SCR with NH$_3$, on two catalytic beds of Fe-zeolite (EnviNOx® process [6]).

Fe-exchanged MFI, *BEA, and FER have been extensively investigated for N_2O abatement reactions [7–25]. For the decomposition, these catalysts were poorly active when compared with other transition metal ions (tmi) in the same zeolites [8]. The widely accepted mechanism involves N_2O adsorption yielding activated oxygen form (O_{ads}^*) and N_2 evolution, and a subsequent removal of O_{ads}^* by O_2 desorption. The latter step was generally considered as rate determining [7–9,15,26], as in fact the activity for N_2O abatement was highly improved by NO addition, acting as an oxygen transporter [26], or by the addition of a hydrocarbon as reductant [20,23,24,27]. For the SCR of N_2O with CH_4 in the presence of oxygen (SCR_{N_2O}) methane was found to be an efficient reducing agent on Fe-MFI [24], Fe-BEA [28,29] and Fe-MOR [11]. On Fe-BEA, the identification of CH_4-deriving intermediates (methoxy and formate) by FTIR during the (SCR_{N_2O}) suggested the removal of the atomic oxygen by hydrocarbon [29]. The features of sites able to activate N_2O and to favor the oxygen removal is still under debate. The tmi active sites, whose location and nuclearity depended strongly on the distribution of Al atoms in the zeolite [30], were reported as mononuclear iron on Fe-MFI [27,31], as dinuclear species on MFI and *BEA matrices [14,15,28,32,33] or as couple of bare Fe^{2+} ions at a proper distance on FER [12,34].

Besides iron, other transition metal ions (tmi) exchanged in zeolites, as cobalt and nickel, were also investigated for N_2O abatement reactions. Co-MFI and Co-MOR were active for both N_2O decomposition and reduction [8,11,35,36]. For decomposition, in these catalysts the O_2 desorption occurred *via* interaction of O_{ads}^* with gaseous N_2O (Eley–Rideal mechanism) [7,9,36,37]. In Co-MFI [36] and Co-MOR [37], isolated mono-atomic Co^{2+} were active sites, whereas dimeric species did not contribute to the activity. In Co-MOR we found that all isolated Co^{2+} activated N_2O by a first oxidative step forming $Co^{3+}O^-$ intermediates (*in situ* UV–vis DRS evidence) [38]. Co-MOR catalysts were also active for (SCR_{N_2O}) [11]. Differently from decomposition, the reaction rate of the (SCR_{N_2O}) correlated with the amount of the isolated Co^{2+} located in the MOR small channels, suggesting these species as the active sites. A possible poisoning of sites in the MOR main channels by the species formed from activated CH_4 was proposed [38]. Further spectroscopic investigations of intermediates during the reaction (*operando* conditions), giving information on the reaction pathway, could better clarify the location of active sites and the possible poisoning.

Differently from iron and cobalt, Ni-MFI [8] and Ni-MOR [38] catalysts, were inactive for N_2O decomposition, whereas Ni-MOR catalysts were highly active for (SCR_{N_2O}), suggesting that CH_4 had a key role for N_2O abatement [38]. The spectroscopic characterization of these samples revealed a high amount of $[Ni^{2+}-O-Ni^{2+}]$ dimers together with isolated Ni^{2+} (*in situ* FTIR characterization), both forming no $Ni^{3+}O^-$ intermediates (*in situ* UV–vis DRS evidence). We concluded that Ni^{2+} were inactive for N_2O decomposition because of Ni^{2+}/Ni^{3+} unsuitable redox properties. For (SCR_{N_2O}) we suggested that the active sites could be $[Ni^{2+}-O-Ni^{2+}]$ dimers in the main channels, but a further spectroscopic investigation was however required to prove it.

To clarify the role of the redox behavior, nuclearity and location of active sites in determining the activity for N_2O decomposition (Co≫Ni) or reduction (Ni > Co) we extended the comparison to Fe-MOR. This catalyst contained a large fraction of exposed iron, as isolated species and/or oligomers at the exchanging sites and was found more active for (SCR_{N_2O}) than Co- and Ni-MOR ones [11]. In the present paper we compared the catalytic activity of Co-MOR, Fe-MOR and Ni-MOR catalysts for the reactions of N_2O abatement (decomposition in the absence or in the presence of NO, and catalytic reduction with CH_4 in the absence of oxygen, CR_{N_2O}, or in the presence of oxygen, SCR_{N_2O}) and for CH_4 combustion. We characterized Fe-MOR by means of *in situ* UV–vis DRS and FTIR characterization, to be compared with Co-MOR and Ni-MOR previously studied [11,39], investigating the reactivity of the active sites with probe molecules (N_2O, NO). On all catalysts, we carried out *operando* FTIR experiments during N_2O decomposition, CR_{N_2O} and SCR_{N_2O} to identify the species formed on the working surface. The

correlation between characterization and catalytic activity results allowed an insight into the nature of active sites and into the reaction pathways of the N_2O abatement.

2. Experimental

2.1. Catalysts

Co-MOR, Fe-MOR and Ni-MOR were portions of those previously prepared [11,39,40]. In Na-MOR matrix (Si/Al = 9.2, Tosoh Corporation), the analytical Na content equaled the Al calculated from the analytical Si/Al ratio given by the supplier. Details on the impurity in MOR matrix are reported in full in a previous paper [39]. Co-MOR, Fe-MOR and Ni-MOR catalysts were prepared by ion-exchange, by contacting a weighted amount of Na-MOR with an aqueous solution (< 0.01 M) of $Co(CH_3COO)_2$, $FeCl_3$, or $Ni(NO_3)_2$ for 6 h under stirring at 350 K. To obtain extensively exchanged samples, up to three exchange procedures were run in sequence. After the exchange procedure, specimens were thoroughly washed with distilled water, dried overnight at 383 K, and called hereafter *as prepared, a.p.,* samples.

The sodium, the cobalt, the iron and the nickel content of wet samples (equilibrated at ca. 79% relative humidity over a saturated solution of NH_4Cl) were determined by atomic absorption (Varian SpectrAA-220) and expressed as Na^+/Al and $n \cdot tmi^{n+}/Al$ ratios, where $n \cdot tmi^{n+}/Al$ is $2 \cdot Co^{2+}/Al$, $3 \cdot Fe^{3+}/Al$, or $2 \cdot Ni^{2+}/Al$, depending on the catalyst. Exchanged samples are labeled as tmi-MOR-*a*, where *a* is the analytical tmi-exchange percentage (Table 1).

The *a.p.* samples were *standard activated (s.a.)* (i) for *in situ* measurements by evacuating from room temperature (RT) to 773 K, heating in O_2 (SOL, 99.9%) at 773 K for 1 h and evacuating at the same temperature for 1 h, or (ii) for measurements under flow by feeding 2.5% O_2/He mixture (100 $cm^3 min^{-1}$) from RT to 773 K and then maintaining isothermally at 773 K for 90 min.

2.2. Catalytic experiments

The catalytic activity was measured in a flow apparatus at atmospheric pressure in steady state conditions. The apparatus included a feeding section where four gas streams (He, 3% N_2O in He, 1.5% CH_4 in He, 10% O_2 in He) were regulated by means of independent mass flow controller-meters (MKS) and mixed in a glass ampoule before entering the reactor. Gas mixtures were purchased from RIVOIRA and used without further purification. The reactor was made of silica with an internal sintered frit of about 12 mm diameter supporting the powdered catalyst. Reactants and products were analyzed by a gas-chromatograph (Agilent 7890 A GC system) equipped with three columns (Molsieve 5 A, for detecting O_2, N_2 and CO, Porapack Q for detecting CO_2 and N_2O, and Na_2SO_4-doped alumina for detecting CH_4) and two detectors (TCD and FID). Experiments yielded satisfactory nitrogen and carbon balances (within the experimental error). In selected experiments we quantify H_2 by using a Varian Micro-GC CP-4900 (N_2 carrier, Mol-Sieve

Table 1

Co-, Fe-, or Ni-exchanged MOR: analytical iron, cobalt, nickel and sodium amounts.

Catalysts	Na^+/Al	$n \cdot tmi^{n+}/Al$[a]
Co-MOR-11	0.91	0.11
Co-MOR-23	0.79	0.23
Co-MOR-41	0.57	0.41
Co-MOR-73	0.32	0.73
Co-MOR-89	0.26	0.89
Fe-MOR-64	0.41	0.64
Ni-MOR-80	0.24	0.80

[a] $n \cdot tmi^{n+}/Al$ is $2 \cdot Co^{2+}/Al$, $3 \cdot Fe^{3+}/Al$, or $2 \cdot Ni^{2+}/Al$, depending on the catalyst.

5 A column and TCD detector).

A portion of *a.p.* sample (0.100 g) was *standard activated*. After this treatment, the reactor was bypassed and the temperature adjusted to the desired value. In a typical catalytic run the reaction temperature was changed at random without intermediate activation treatment. Catalysis was run by contacting the catalyst with mixtures of various composition (v/v, He as balance): N_2O, $N_2O + NO$, $N_2O + CH_4$ (CR_{N_2O}), $N_2O + CH_4 + O_2$ (SCR_{N_2O}) and $CH_4 + O_2$. The concentration was 4000 ppm for N_2O, NO and CH_4 and 20,000 ppm for O_2, with He as balance. The total flow rate was maintained at 50 cm^3 STP/min, and space velocity (GHSV) was 15,000 h^{-1}, based on the apparent sample density of 0.5 g cm^{-3}. For all reactions, the catalyst was stable as a function of the time on stream, throughout experiments lasting up to about 8 h. Conversions obtained at various (sample weight)/(flow rate) ratios (W/F) indicated that, in our conditions, reaction is under kinetic control without diffusion effect.

Percent N_2O or CH_4 conversion was calculated as 100·(molecules consumed)/(molecules injected). Percent CO_2 selectivity, S_{CO_2}, was calculated as 100·(CO_2 formed)/($CO_2 + CO$ molecules formed). Percent H_2 yield was calculated as 100·(½H_2 molecules formed)/(CH_4 molecules consumed). For each catalyst, specific reaction rate (R / molecules $s^{-1} g^{-1}$) for N_2O reduction and apparent activation energy values (E_a / kJ mol^{-1}) were calculated from experiments in which conversion values did not exceed 30% (log R *vs.* 1/T).

The N_2O/CH_4 ratio was calculated as (N_2O molecules consumed)/ (CH_4 molecules consumed) and the O_2/CH_4 ratio as (O_2 molecules consumed)/(CH_4 molecules consumed). We discussed the reaction stoichiometry of the CR_{N_2O} on the basis of the following reactions:

$$CH_4 + 4N_2O \rightarrow 4N_2 + CO_2 + 2H_2O \qquad (a)$$

$$CH_4 + 3N_2O \rightarrow 3N_2 + CO + 2H_2O \qquad (b)$$

$$CH_4 + 2N_2O \rightarrow 2N_2 + CO_2 + 2H_2 \qquad (c)$$

$$CH_4 + N_2O \rightarrow N_2 + CO + 2H_2 \qquad (d)$$
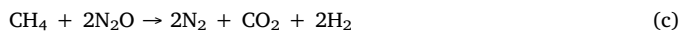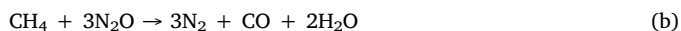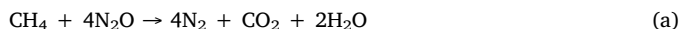
2.3. Characterization techniques

In situ UV–vis DRS spectra were recorded on Fe-MOR at RT in the wavenumber range of 4000–50000 cm^{-1} using a Varian Cary 5E spectrometer (software Cary Win UV). The spectra were run *in situ* in a quartz cell with optical windows, that allowed thermal treatments in vacuum or in a controlled atmosphere. The spectra were recorded on sample (about 1.0 g) (i) *a.p.* in air, (ii) *s.a.*, (iii) *s.a.* and exposed to NO (AIR LIQUIDE/SIO, 99.0%), (iv) *s.a.*, heated in CO (SOL, 99.9%) at increasing temperature up to 473 K, cooled in CO at RT, evacuated at RT and exposed to NO or (v) *s.a.*, heated in N_2O (SOL, 99.9%) at increasing temperature up to 773 K, for 10 min at each temperature, and cooled in N_2O at RT.

FTIR spectra were recorded on all catalysts by a spectrometer Perkin Elmer Frontier, equipped with a MCT detector, operating at a resolution of 4 cm^{-1}. The powdered samples were pelleted (pressure, 2×10^4 kg cm^{-2}) in self-supporting wafers of about 20 mg (10 mg cm^{-2}). For *in situ* measurements with probe molecules, samples were put in a quartz cell, provided with KBr windows, which allowed thermal treatments in vacuum or in a controlled atmosphere. Before adsorption of NO or N_2O catalysts were activated. For the *operando* FTIR experiments, sample pellets were put in a stainless-steel reactor, equipped with CaF_2 windows, that allowed to record spectra up to 773 K, under gas stream. The IR reactor was connected to the flow apparatus we used for catalytic measurements, and reactants and products were analyzed by the on-line gas-chromatograph. Samples were *standard activated*, cooled to the desired temperature under He flow, and exposed to the feeding mixtures, having the same composition as that we used for catalytic experiments. Spectra were recorded at increasing temperature. The catalytic data of the *operando* experiments were in agreement with those
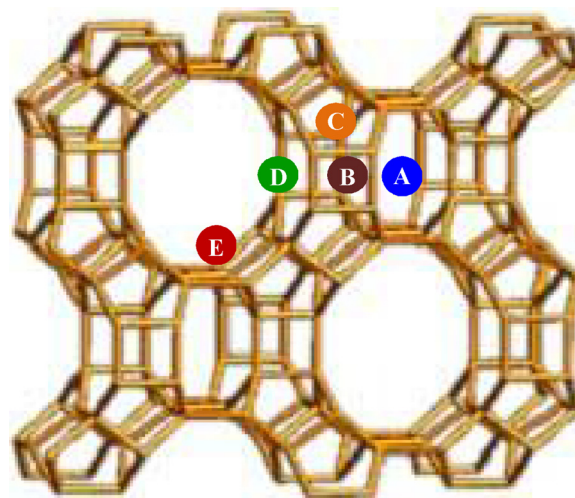

Fig. 1. Framework and cationic location in dehydrated MOR, according to Refs. [41–44].

yielded in the plug-flow reactor. For selected cases, we recorded spectra as a function of time on stream at a constant temperature, and we carried out experiments by changing the addition order of the reactants (N_2O and CH_4), namely pre-saturating the surface with one reactant and subsequently adding the other one. Spectra recorded after heating samples in the He stream at a given temperature (blank experiments at 298–773 K) were subtracted from those obtained after heating in the reactant mixture stream at the same temperature.

3. Results and discussion

3.1. The oxidation state, nuclearity and location of transition metal ion in MOR

In MOR, monovalent exchangeable cations were located on the wall of the main channels (E sites), in the small channels (A sites), near the entrance of the interconnecting side pockets (D sites) or inside the side pockets (B or C sites) [41–44] (Fig. 1). When these sites were in pairs at the proper distance, they were exchangeable with isolated divalent tmi species [30]. The tmi dimeric species, whose charge depended on their structure, were expected to be located in the main channels or in the interconnecting side pockets, for their steric hindrance [45].

In Fe^{3+}-exchanged zeolites, the ion-exchange stabilized a variety of iron species with different nuclearity, because (i) mononuclear trivalent cations were difficulty balanced by the localized negative charge of zeolite framework and (ii) mononuclear Fe^{3+} aquo-complexes in aqueous solution hydrolyzed and condensed in dimeric and polynuclear hydroxo-complexes [46,47]. Several authors found that in Fe-ZSM-5, Fe-BEA and Fe-silicalite, after evacuation at high temperature, Fe^{3+} partially reduced to coordinatively unsaturated sites (c.u.s.) Fe^{2+} [31,48–50]. In particular, in Fe-ZSM-5 and in Fe-silicalite, evacuated at high temperature and exposed to NO, Zecchina et al. [50] evidenced Fe^{2+}-$(NO)_x$ species, thanks to their high extinction coefficient (UV–vis absorption in the region 10,000–30,000 cm^{-1}). The formation of Fe^{2+} species was generally ascribed to the so called "auto-reduction" of Fe^{3+} during high temperature evacuation [33,51,52]. For zeolites synthesized with organic templates, the residual C species contributed to the tmi reduction during evacuation at high temperature, as demonstrated for Cu-MFI by Occhiuzzi et al. [53]. As MOR synthesis does not involve organic templates, the Fe^{3+} reduction to Fe^{2+} species during high temperature evacuation could not be explained with residual carbon species.

In situ UV–vis DRS spectrum of *a.p.* Fe-MOR-64 (Fig. 2a) sample showed bands at about 49,000 and 36,000 cm^{-1}, due to ligand-to-metal
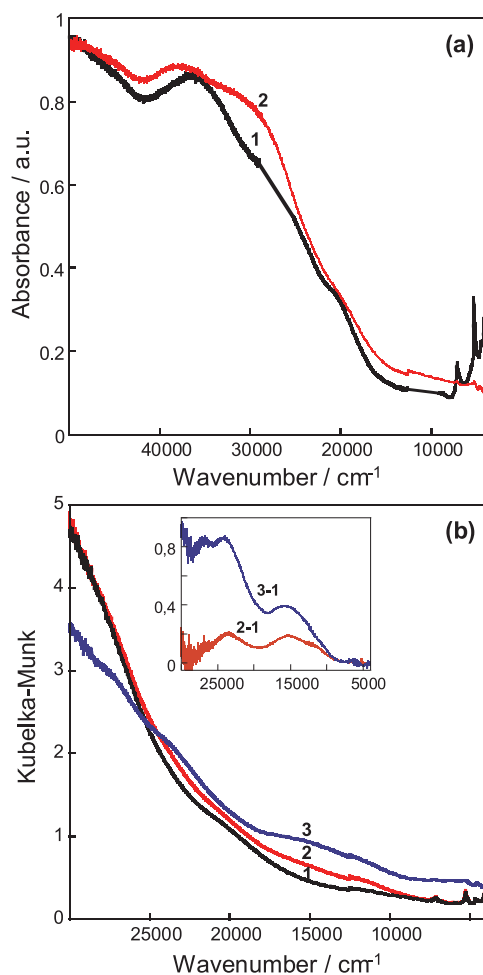
Fig. 2. *In situ* UV–vis DRS spectra of Fe-MOR-64 catalyst. Section a: *as prepared* sample under air atmosphere (1), and *standard activated* (2). Section b: *standard activated* sample (1); *standard activated* and exposed to NO (100 Torr) at RT (2); *standard activated*, heated in CO at 473 K, evacuated at room temperature and exposed to NO (100 Torr) at RT (3). The inset in Section b reports the two differences in the d-d region: spectrum 3 – spectrum 1 (3–1) and spectrum 2 – spectrum 1 (2–1).

O–Fe charge-transfer transitions of octahedral Fe^{3+} aquo-complexes, and low absorption at about $20,000 \, cm^{-1}$, due to Fe^{3+} oligomers [27,47,50]. In *s.a.* sample the spectrum showed intense bands at $48,000 \, cm^{-1}$ and $38,200 \, cm^{-1}$, due to Fe^{3+} in tetrahedral and octahedral configurations, and broad adsorption in the $33,000–28,000 \, cm^{-1}$ region, due to small oligonuclear Fe_xO_y clusters [27]. In agreement with Zecchina et al. [50], NO adsorption on *s.a.* sample (Fig. 2b) yielded new bands in d-d region $10000-30000 \, cm^{-1}$, well evidenced in the difference spectrum ($25,000$ and $15,000 \, cm^{-1}$ with a shoulder at $12,000 \, cm^{-1}$, see inset in Fig. 2b), that were typical of *pseudo-octahedral* Fe^{2+}-(NO)$_x$ complexes [50,54]. Being no organic templates used in MOR synthesis, the formation of the c.u.s. Fe^{2+} species can be due to the removal of the extra-lattice oxygen atoms in [Fe^{3+}-O-Fe^{3+}] species by high-temperature treatments. Due to their steric hindrance, the Fe^{3+} dimers were possibly located in main channels of MOR or in the interconnecting side pockets. To better characterize the reducibility of Fe^{3+} dimers, the *s.a.* Fe-MOR-64 sample was reduced in CO at 473 K. After subsequent exposure to NO at RT (Fig. 2b), the Fe^{2+}-(NO)$_x$ d-d bands showed an intensity higher than that detected in *s.a.* sample with an additional component at $27,000 \, cm^{-1}$ (compare spectra 3-1 and 2-1 in the inset of Fig. 2b), indicating the presence of a second type of Fe^{2+} species. The two families of Fe^{2+} dimeric species, formed by reduction of two types of Fe^{3+} dimers having a different stability of extra-lattice oxygen,
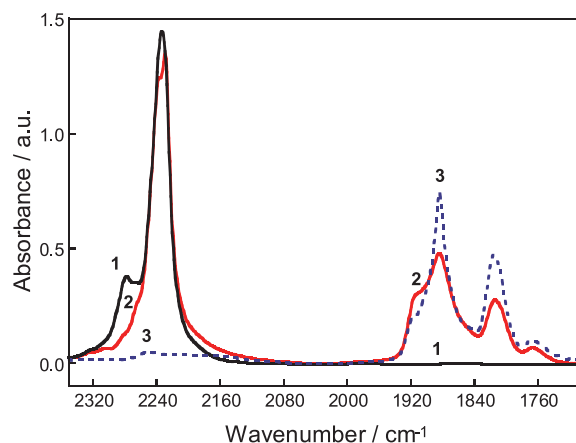
possibly differed in terms of coordination in the MOR cages. Similarly, two families of active [Cu–O–Cu]$^{2+}$ sites precursor for Cu^+ dimers were found in Cu-MOR [45].

In situ FTIR characterization of *s.a.* Fe-MOR-64 confirmed the formation of c.u.s. Fe^{2+} sites in MOR. In fact, the spectra of *s.a.* sample exposed to N_2O at RT showed bands at $2278 \, cm^{-1}$ and at $2233 \, cm^{-1}$ (spectrum 1 in Fig. 3), that were assigned to N_2O adsorbed on Fe^{2+} and on matrix sites, respectively [10,31]. After the subsequent NO addition (spectrum 2 in Fig. 3), the band at $2278 \, cm^{-1}$ disappeared, while bands due to stretching modes of Fe^{2+}-(NO)$_x$ (x from 2 to 3) on well dispersed iron species and of mono-nitrosyls on oligomers ($1950–1750 \, cm^{-1}$ region) formed, similar to those observed without N_2O pre-adsorption (Fig. 3, spectrum 3). The disappearance of the band at $2278 \, cm^{-1}$ indicated that N_2O and NO competed for the same Fe^{2+} sites and that the Fe^{2+}-N_2O complexes were less stable than the Fe^{2+}-nitrosyl ones.

As concerns Co-MOR and Ni-MOR [38–40], we have previously reported that both catalysts contained tmi^{2+} in octahedral configuration in *a.p.* samples, and in a distorted tetrahedral configuration in *s.a.* samples (*in situ* UV–vis DRS evidence). In *s.a.* samples, we have found, by *in situ* FTIR evidence, that: (i) Co^{2+} species were mainly dispersed as isolated ions in both main and small channels of MOR, being [Co^{2+}-O-Co^{2+}] dimers amount up to about 10% of exchanged Co in the most concentrated sample (Co-MOR-89), and (ii) Ni^{2+} species were present as isolated Ni^{2+} and [Ni^{2+}-O-Ni^{2+}] dimers, the latter in an amount much higher than in Co-MOR, *i.e.* up to about 50% in the most concentrated sample (Ni-MOR-80).

3.2. N_2O decomposition on tmi-MOR

3.2.1. Catalytic activity for N_2O decomposition in the absence and in the presence of NO

For N_2O decomposition (Fig. 4, open symbols), Co-MOR and Fe-MOR catalysts were active, whereas Ni-MOR was inactive. The N_2O conversion for Co-MOR-73 started at about 573 K and reached about 100% at 773 K (Fig. 4a); for Fe-MOR-64 it started at about 700 K and reached 68% at 773 K (Fig. 4b); for Ni-MOR-80 it was < 5% at 773 K (Fig. 4c). The results on both Co-MOR-73 and Ni-MOR-80 matched those we previously reported [38].

After NO addition to N_2O feed (Fig. 4, closed symbols), the N_2O conversion did not change on Co-MOR-73 and Ni-MOR-80, whereas it markedly increased on Fe-MOR-64, starting at about 125 K lower temperature and reaching about 100% at 723 K (compare closed with open square in Fig. 4). Since NO remained unconverted, on Fe-MOR-64 it played a catalytic role in the N_2O decomposition mechanism, as reported for Fe-MFI catalysts [26,55,56].
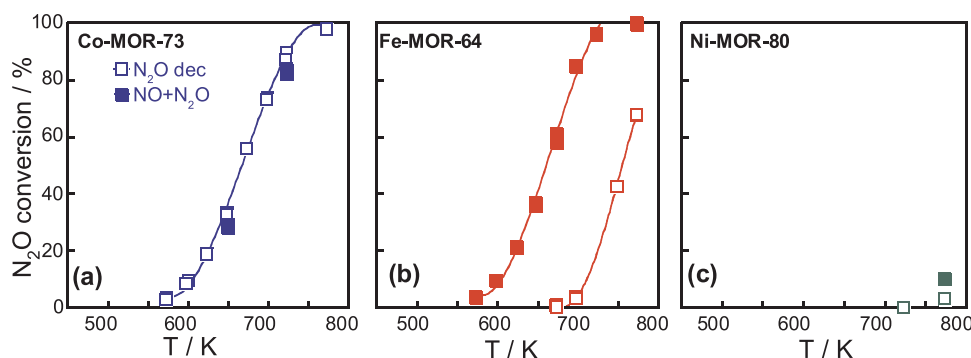
Fig. 4. N_2O decomposition in the absence (open symbols) and in the presence of NO (closed symbols). Percent N_2O conversion as a function of temperature on Co-MOR-73 (Section a), Fe-MOR-64 (Section b), Ni-MOR-80 (Section c). Reactant concentration: $[N_2O]$ = [NO] = 0.4% (total flow rate = 50 cm^3 STP/min, He as balance).

3.2.2. The redox behavior of transition metal ion in the reactant mixture

To clarify the tmi redox behavior during N_2O decomposition, we heated tmi-MOR samples in N_2O at increasing temperature and characterized them by *in situ* UV-vis DRS. In our previous paper we found that the heating in N_2O at increasing temperature (423–723 K) on Co-MOR yielded the formation of Co^{3+}-O^-, whose amount increased with temperature increase, whereas on Ni-MOR it yielded no Ni^{2+} oxidation [38].

On Fe-MOR-64 the heating in N_2O at increasing temperature (Fig. 5) yielded an intensity change of the bands of Fe^{3+} in tetrahedral and octahedral configurations (48,000 and 38,200 cm^{-1}): from 298 to 623 K, where the sample was inactive for N_2O decomposition (see Fig. 4b), their intensity increased (spectra 1 to 3 in Fig. 5), whereas at 773 K, where the sample was active, their intensity decreased (spectrum 4 in Fig. 5). The intensity change of these bands suggested a Fe^{2+}/Fe^{3+} redox cycle during the heating in N_2O. The increase of Fe^{3+} bands up to 623 K was due to the oxidation of the Fe^{2+} species in *s.a.* sample by the oxygen atom released from N_2O, possibly yielding a stable intermediate, thus accounting for the sample inactivity. The subsequent decrease of Fe^{3+} bands at higher temperature was due to the reduction of this intermediate, thus accounting for sample activity.

To investigate the surface species formed on tmi-MOR during N_2O decomposition in the absence or in the presence of NO, *operando* FTIR experiments were carried out (Fig. 6). On Co-MOR-73 (Fig. 6a) during the N_2O decomposition just a small amount of nitrites/nitrates (1590–1450 cm^{-1} region) formed, that might arose as by-products from N_2O disproportionation on [Co^{2+}-O-Co^{2+}] dimeric species, inactive for decomposition [37]. In the OH region (spectral region not shown) the parallel detection of a negative peak at 3650 cm^{-1} with a
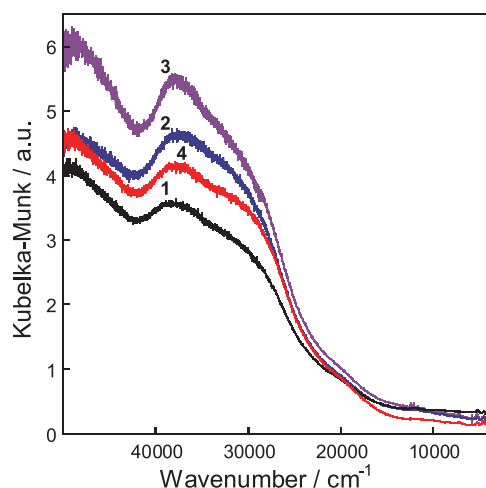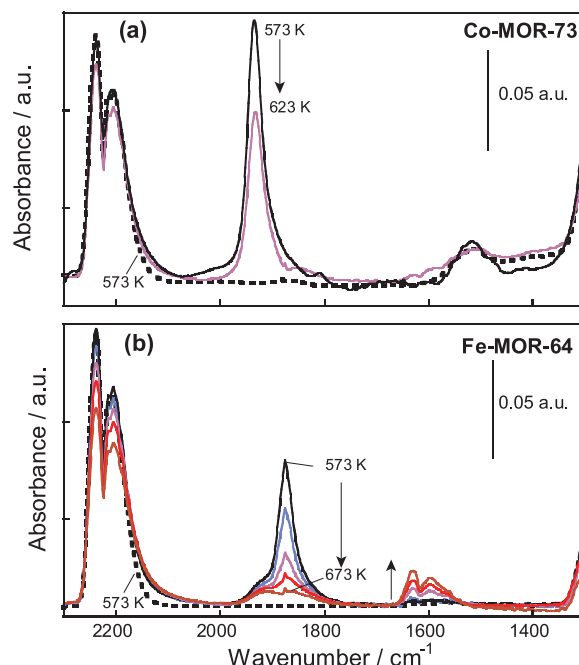

Fig. 6. *Operando* FTIR spectra of surface species on *standard activated* Co-MOR-73 (Section a) and Fe-MOR-64 (Section b) after saturation under N_2O flow at 573 K (dotted line spectra), under (N_2O + NO) flow at the same temperature (bold line spectra) and at increasing temperature, as indicated. Reactant concentration: $[N_2O]$ = [NO] = 0.4%, (total flow rate = 50 cm^3 STP/min, He as balance).

nearby positive absorption at lower wavenumber suggested the interaction of nitrites/nitrates with an adjacent Co^{2+}-OH species on dimers. The addition of NO to N_2O feed at increasing temperature, yielding no change in N_2O conversion, caused the formation of Co^{2+}-nitrosyls, and no significant change in the amount of nitrites/nitrates. Increasing the reaction temperature, the intensity of both Co^{2+}-nitrosyl and nitrites/nitrates bands decreased, as expected for their thermal stability.

On Fe-MOR-64 (Fig. 6b), during N_2O decomposition no formation of surface species was detected. After the addition of NO to N_2O feed the spectrum at 573 K showed Fe^{2+}-nitrosyls (bands at 1876 cm^{-1} with a shoulder at about 1920 cm^{-1} [57]) and little amount of nitrites/nitrates on iron sites and/or on matrix sites (bands at about 1620 and 1590 cm^{-1}). Increasing the temperature up to 673 K, at which decomposition occurred (N_2O conversion 19% in the *operando* experiment), the intensity of Fe^{2+}-nitrosyl bands decreased whereas that of nitrites/nitrates bands increased, suggesting the oxidation of NO during the N_2O decomposition.

On the inactive Ni-MOR-80 (spectra not shown), showing no surface species under N_2O feed at 773 K, the addition of NO (no change in N_2O conversion) caused the formation of Ni^{2+}-nitrosyls alone, whereas no
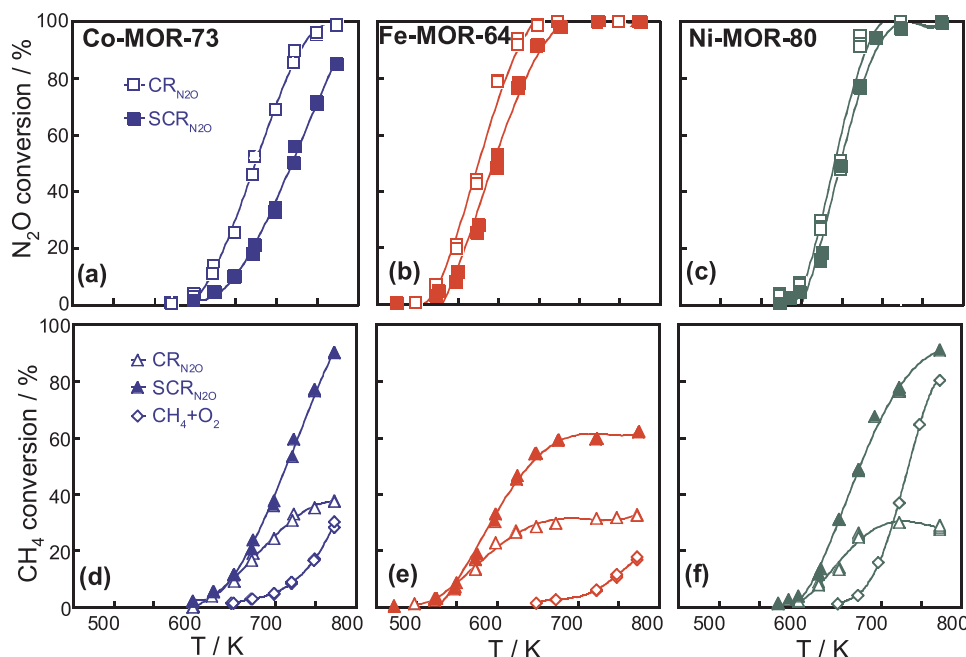

Fig. 5. *In situ* UV–vis DRS spectra at RT of *standard activated* Fe-MOR-64 catalyst exposed at RT to N_2O (225 Torr, spectrum 1), and heated in N_2O at increasing temperature: 523 K (spectrum 2), 623 K (spectrum 3) and 773 K (spectrum 4).

Fig. 7. Comparison between CR_{N_2O}, SCR_{N_2O} and CH_4 combustion on Co-MOR-73 (Section a and d), Fe-MOR-64 (Section b and e) and Ni-MOR-80 (Section c and f): percent N_2O conversion (Sections a–c) and percent CH_4 conversion (Sections d–f) as a function of temperature. Reactions as indicated. Reactant concentration: $[N_2O] = [NO] = 0.4\%$, $[O_2] = 2\%$ (total flow rate = 50 cm^3 STP/min, He as balance).

nitrites/nitrates formed.

### 3.2.3. Reaction pathway and active sites for N_2O decomposition

On Co-exchanged zeolites, for N_2O decomposition we have previously proposed the "cationic redox mechanism" [37]. In the first oxidative step isolated Co^{2+} species acted as electron-donor center toward the anti-bonding orbital of N_2O:

$$N_2O + Co^{2+} \rightarrow N_2 + Co^{3+}O_{ads}^- \tag{1}$$

The second step consisted of tmi reduction as a result of oxygen desorption, that occurred on isolated sites via Eley-Rideal (E–R) mechanism:

$$Co^{3+}O_{ads}^- + N_2O \rightarrow N_2 + O_2 + Co^{2+} \tag{2}$$
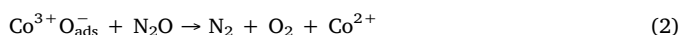
In this paper we found that the cationic redox mechanism was also operative on Fe-MOR-64 catalyst. We detected c.u.s. Fe^{2+} on *s.a.* sample (UV–vis DRS and FTIR evidence). These c.u.s. Fe^{2+}, whatever their nuclearity and structure (isolated or poly-nuclear), had the proper oxidation state to activate N_2O, yielding oxidation to Fe^{3+} (UV–vis DRS evidence) and adsorbed activated oxygen species (hereafter called O_{ads}^*). The desorption of O_2 in the second step, which was generally recognized as the rate determining step [7–9,15,26], may occur by reaction of O_{ads}^* with a second N_2O molecule (Eley-Rideal, E-R, mechanism) or by recombination of two O_{ads}^* intermediates (Langmuir-Hinshelwood, L-H, mechanism). The low activity of Fe-MOR-64 for N_2O decomposition in the absence of NO suggested a low reactivity of surface O_{ads}^* species to realize the second step. We supposed therefore that the c.u.s. Fe^{2+} active for the decomposition belonged to dimeric $[Fe^{2+}-\square-Fe^{2+}]$ species, formed during the *s.a.* treatment by reduction of a fraction of dimeric Fe^{3+} species and possibly located in the main channels. This dimeric species reacted with N_2O oxidizing to $Fe^{3+}-O^{(1+\delta)-}—Fe^{(2+\delta)+}$:

$$Fe^{2+}-\square-Fe^{2+} + N_2O \rightarrow N_2 + Fe^{3+}-O^{(1+\delta)-}—Fe^{(2+\delta)+} \tag{3}$$
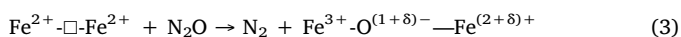
This intermediate species had a high stability (UV–vis DRS evidence, see Fig. 5), due to the quasi-oxidic character of the bridged oxygen interacting with two tmi. Therefore, the second step required

either (i) high temperature to desorb oxygen via E–R mechanism,

$$Fe^{3+}-O^{(1+\delta)-}—Fe^{(2+\delta)+} + N_2O \rightarrow N_2 + O_2 + Fe^{2+}-\square-Fe^{2+} \tag{4}$$
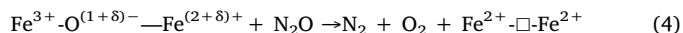
or (ii) the addition of an O-scavenger, to desorb oxygen via L-H mechanism. The NO added to the feed acted as a means of transport for oxygen atoms, reacting with the stable $Fe^{3+}-O^{(1+\delta)+}—Fe^{(2+\delta)+}$ intermediates and yielding nitrites/nitrates species (*operando* FTIR evidence, see Fig. 6). The adsorbed nitrites/nitrates species subsequently restored NO, via pairing with another oxygen species adsorbed on nearby site, as proposed by Perez-Ramirez et al. on Fe-MFI [26,55].

The unchanged activity of the active Co-MOR-73 after NO addition to the feed can be due to the high reactivity of $Co^{3+}-O^-$ species towards a second gaseous N_2O molecule, not requiring NO as O-scavenger. The oxyl character of oxygen in $Co^{3+}-O^-$ intermediate with respect to the quasi-oxidic character of oxygen in the $Fe^{3+}-O^{(1+\delta)-}—Fe^{(2+\delta)+}$ accounted for its higher activity.

On Ni-MOR-80, where no N_2O decomposition occurred, neither isolated Ni^{2+} nor dimeric species were oxidized by N_2O (Uv–vis DRS evidence [38]). Therefore, the first step of cationic redox mechanism did not occur and NO addition to the feed had no effect.

On the whole, key factors for N_2O decomposition activity are the formation and the stability of O_{ads}^* surface species, both affected by the mobility of the tmi electrons. In particular, the formation of activated oxygen required a partial or a total electron transfer from tmi, whereas the oxygen desorption via E–R or via L-H mechanism required a partial or a total electron transfer toward tmi.

3.3. N_2O reduction with CH_4 on tmi-MOR

3.3.1. Catalytic activity for N_2O reduction with CH_4 in the absence and in the presence of O_2

For N_2O reduction with CH_4 in the absence of O_2 (CR_{N_2O}) all catalysts were highly active (Fig. 7). N_2O conversion reached 100% at different temperature on each catalyst (on Co-MOR-73 at 750 K, on Fe-MOR-64 at 650 K, on Ni-MOR-80 at 670 K), while CH_4 conversion was about 30-40%. The catalysts had a similar apparent activation energy ($E_a = 120 \pm 10$ kJ mol^{-1}), and the activity order, evaluated by the comparison of specific rates, was Fe-MOR-64 > Ni-MOR-80 > Co-
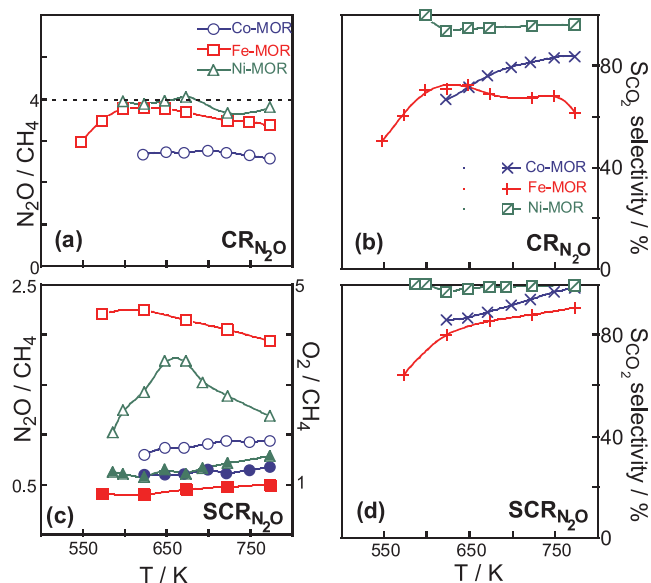
Fig. 8. Reactant conversion ratios and CO_2 selectivity in CR_{N_2O} and SCR_{N_2O} reactions on Co-MOR-73, Fe-MOR-64 and Ni-MOR-80 catalysts. N_2O/CH_4 ratio (Section a and c, open symbols), O_2/CH_4 ratios (Section c, closed symbols) and S_{CO_2} (Section b and d) as a function of temperature. Catalysts and reactions as indicated.

MOR-73.

On the three catalysts the CR_{N_2O} process might occur *via* reactions a–d listed in Section 2.2; the N_2O/CH_4 ratio combined with the selectivity to CO_2 (S_{CO_2}) indicated if parallel reactions occurred (Fig. 8a and b). On Ni-MOR-80 the N_2O/CH_4 ratio as a function of temperature was nearly constant at about 4 (Fig. 8a), *i.e.* the stoichiometric ratio of the reaction a, and in agreement S_{CO_2} was ≥95% in the whole temperature range (Fig. 8b). On Co-MOR-73 and on Fe-MOR-64, the N_2O/CH_4 ratio was lower than 4 (about 2.7 on Co-MOR-73 and 3.0–3.8 on Fe-MOR-64), indicating that the other reactions had to be considered. Due to the fact that S_{CO_2} was higher than 50% in the whole temperature range (Fig. 8b), the occurrence of the reaction b alone ($N_2O/CH_4 = 3$) yielding CO as product could not justify the N_2O/CH_4 values ≤ 3.5 and therefore side-reactions yielding H_2 (reaction c and d) had to be taken into account. In agreement, on Co-MOR-73 GC analysis during CR_{N_2O} revealed H_2 in the outlet mixture, whose yield increased with temperature (up to 10% at 773 K). In Co-MOR-73 the low value of N_2O/CH_4 suggested that no N_2O decomposition occurred in parallel to reduction. As C and N balances were equal to 100%, reactions yielding other by-products were excluded.

For N_2O reduction with CH_4 in the presence of O_2 (SCR_{N_2O}) all catalysts were active (Fig. 7), the N_2O and the CH_4 conversions matched those we previously found [11] and the activity order for SCR_{N_2O} was the same as CR_{N_2O}. The comparison of SCR_{N_2O} with CR_{N_2O} showed that the presence of O_2 in the gas feed (i) lowered the N_2O conversion in Co-MOR-73 and Fe-MOR-64 (Fig. 7a and b), whereas leaved unchanged that in Ni-MOR-80 (Fig. 7 c), and (ii) increased CH_4 conversion on all catalysts (Fig. 7d, e and f), markedly on Co-MOR-73 and Ni-MOR-80, slightly on Fe-MOR-64. As we previously reported [11], on all samples the reduction yielded CO_2 alone (S_{CO_2} > 90%, Fig. 8d). Since on Co-MOR-73 and Fe-MOR-64 both the N_2O/CH_4 and O_2/CH_4 ratios were constant in the whole temperature range (Fig. 8c), the SCR_{N_2O} reaction occurred on these catalysts with a single stoichiometry, namely $CH_4 + N_2O + 3/2O_2 \rightarrow N_2 + CO_2 + 2H_2O$ for Co-MOR-73, and $CH_4 + 2N_2O + O_2 \rightarrow 2N_2 + CO_2 + 2H_2O$ for Fe-MOR-64. Differently, on Ni-MOR-80 both the ratios were not constant. Since for $CH_4 + O_2$ reaction this catalyst was somewhat active (Fig. 7f), whereas Co-MOR and Fe-MOR were poorly active above 723 K (Fig. 7d and e), on Ni-MOR-80
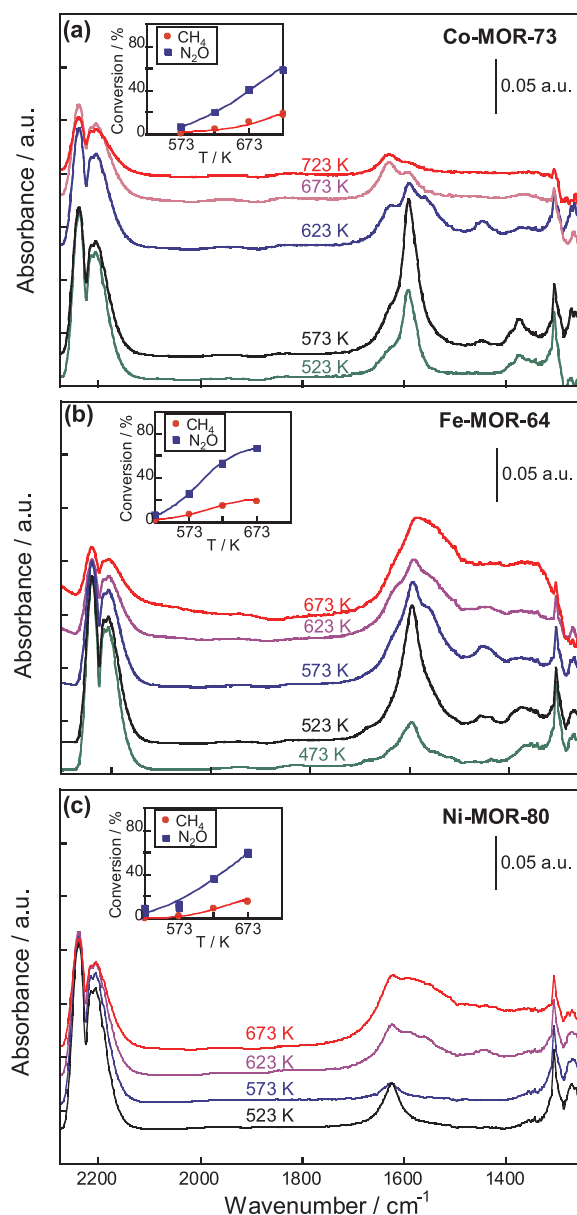

Fig. 9. *Operando* FTIR spectra of surface species during CR_{N_2O} reaction at increasing temperature on *standard activated* Co-MOR-73 (Section a), Fe-MOR-64 (Section b), and Ni-MOR-80 (Section c) catalysts. In the inset, the corresponding reactant conversions as a function of temperature. Reactant mixture: $[N_2O]$ = $[CH_4]$ = 0.4%, (total flow rate = 50 cm³ STP/min, He as balance).

methane combustion possibly occurred as side-reaction during SCR_{N_2O}.

Comparing the stoichiometry of SCR_{N_2O} with that of CR_{N_2O}, on all samples the presence of O_2 caused the decrease of the N_2O/CH_4 ratio, indicating that O_2 competed with N_2O in the oxidative steps of the reaction pathway, in a different extent on each catalyst.

3.3.2. Surface species during N_2O reduction in the absence of O_2 detected by Operando FTIR

On all tmi-MOR, *operando* FTIR experiments during the CR_{N_2O} reaction (see insets in Fig. 9) yielded, in addition to bands of residual gaseous reactants ($CH_{4(g)}$ at 3016 cm⁻¹, and $N_2O_{(g)}$ at 2223 cm⁻¹), bands in the region 1660-1300 cm⁻¹ (Fig. 9). These bands were assigned [29,58,59] to (i) $\nu_{as}(COO)$ (1590 and 1560 cm⁻¹), $\delta(CH)$ (1390 cm⁻¹), and $\nu_s(COO)$ (1375 and 1345 cm⁻¹) of two types of formate, (ii) $\nu(C=O)$ (1625 cm⁻¹) of adsorbed formaldehyde, and (iii) $\delta_{as}(CH_3)$ and $\delta_s(CH_3)$ (1450 cm⁻¹, with a shoulder at 1435 cm⁻¹) of the

methoxy species. These methoxy, formaldehyde and formates (called hereafter CH_xO_y species), arose from consecutive oxidation steps of methane by N_2O. A similar oxidative pathway has been reported in the spectroscopic study of methanol oxidation to CO_2 over V-Ti oxides [58]. The two types of formate species possibly arose from two methoxy species with different reactivity. On Co-MOR-73, the type-I formate band at $1560 \, cm^{-1}$ formed together with the methoxy bands, whereas the type-II formate band at $1590 \, cm^{-1}$ formed at lower temperature together with formaldehyde.

The band intensities of the CH_xO_y species and their changes with temperature were different on each tmi-MOR. In Co-MOR-73 and Fe-MOR-64 (Fig. 9a, b) the CH_xO_y bands were detected at 523 and 473 K respectively, namely before the beginning of the catalytic reaction, and reached their maximum intensity at the light-off temperature (573 and 523 K, respectively). In Co-MOR-73, the CH_xO_y bands decreased with increasing reaction temperature, particularly those due to the type-I formate and to methoxy, whereas the band of the type-II formate was detected up to 723 K, suggesting a higher stability of this species. Differently, in Ni-MOR-80 the CH_xO_y bands were detected at $T \geq 623 \, K$, namely at higher temperature than the reaction light-off (523 K) (Fig. 9c), whereas at lower temperature a band at $1625 \, cm^{-1}$ was detected, that we assigned to incipient adsorbed water (see below). These results suggested a different reaction pathway on Ni-MOR-80.

To gain further information on the CR_{N_2O} reaction pathway, we investigated the formation of species on the surface as a function of time on stream by adding the two reactants one by one, and changing the addition order. On each tmi-MOR we chose the temperature at which band intensities of CH_xO_y intermediates were high enough to investigate their relative change. In particular, we saturated the surface with the first reactant (either N_2O or CH_4), recorded the spectrum (t = 0 min), and then we added the second reactant, recording the spectra at increasing time on stream. The species formed in the first minutes after the second reactant addition depended on the addition order in a different way on each catalyst, whereas those formed at steady state under $N_2O + CH_4$ flow (about 30 min of mixture feeding) did not.

On Co-MOR-73 (Fig. 10a), under CH_4 feed at 623 K no surface species formed, whereas under N_2O feed the spectrum showed the weak bands of nitrites/nitrates ($1500–1600 \, cm^{-1}$), and the weak negative band at $3650 \, cm^{-1}$, due to their interaction with Co^{2+}-OH species (OH spectral region not shown). When the second reactant was added, in the first minutes the addition order had a significant effect. Specifically, the addition of CH_4 to the surface pre-saturated with N_2O ($N_2O + CH_4$) after 1 min of feeding yielded an amount of type-II formate and formaldehyde higher than that obtained after addition of N_2O after pre-saturation with CH_4 ($CH_4 + N_2O$), namely the pre-saturation with N_2O favored methane activation. The parallel intensity increase of both the matrix OH band at $3595 \, cm^{-1}$ (inset in Fig. 10a) and the CH_xO_y bands suggested the H-extraction from CH_4 by c.u.s. $Al-O^-$ [45] with formation of methoxy species. In agreement with Marie et al. [41], the band at $3595 \, cm^{-1}$ can be assigned to matrix OH located in the D sites in the interconnecting side pockets.

On Fe-MOR-64 (Fig. 10b), under single reactant feeding (CH_4 or N_2O) at 573 K no surface species formed (bands due to the gaseous species alone). When the second reactant was added, the addition order had a small effect on the CH_xO_y species formation: in the first 3 min of feeding, the amount of the type-II formate was little higher on a surface pre-saturated with CH_4 ($CH_4 + N_2O$) than on a surface pre-saturated with N_2O ($N_2O + CH_4$). Differently from Co-MOR-73, in the OH region (inset in Fig. 10b) negative bands due to Fe-OH ($3670 \, cm^{-1}$) and to matrix OH in D sites ($3595 \, cm^{-1}$) were detected. The decrease of both OH species bands was possibly due to H-bond between OH and nearby CH_xO_y or to desorption of water formed in the CH_4 activation, as reported by Nobukawa et al. on Fe-BEA [29].

On Ni-MOR-80 (Fig. 10c), under N_2O at 623 K feed no surface species formed, whereas under CH_4 feed the spectrum showed a weak
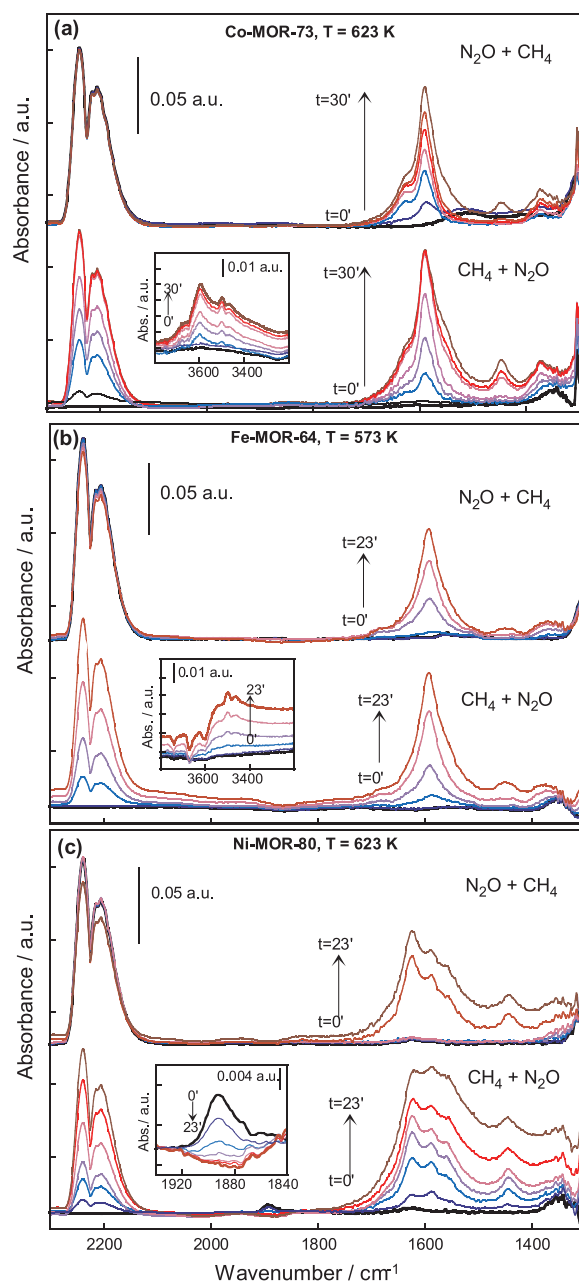

Fig. 10. The effect on surface species of the N_2O and CH_4 addition order to the feed on the *standard activated* Co-MOR-73 (Section a), Fe-MOR-64 (Section b) and Ni-MOR-80 (Section c) catalysts. The FTIR spectra at a constant temperature (above the CR_{N_2O} light-off, as indicated) are recorded at increasing mixing time after pre-saturating the surface with the first reactant (bold dark lines) and the subsequent addition of the second reactant ($N_2O + CH_4$ or $CH_4 + N_2O$, as specified). In the insets, exploded view of the OH stretching region for Co-MOR-73 and Fe-MOR-64, and of the carbonyl stretching region for Ni-MOR-80. Reactant mixture: $[N_2O] = [CH_4] = 0.4\%$ (total flow rate = 50 cm^3 STP/min, He as balance).

band at about $1890 \, cm^{-1}$ (inset in Fig. 10c). As this wavenumber is consistent with bands of carbonyls bridged on electron rich cations, we assigned the peak at $1890 \, cm^{-1}$ to $[Ni^+-(CO)-Ni^+]$ species, that arose from reduction of $[Ni^{2+}-O-Ni^{2+}]$ dimers by methane. On Ni-MOR, the effect of reactant addition order was noticeable. When N_2O was added after pre-saturation with CH_4 ($CH_4 + N_2O$), the Ni^+-carbonyl species disappeared after 5 min of feeding, the CH_xO_y species formed and with increasing feeding time their amount progressively increased. Differently, when CH_4 was added after pre-saturation with N_2O ($N_2O + CH_4$),

no spectral changes were observed for the first 8 min of feeding, whereas after 13 min abrupt formation of formates, methoxy and formaldehyde was observed. In the OH spectral region no absorption changes were observed, except for absorption of H-bonded OH. These results indicated that the Ni^{2+} pre-reduction by CH_4 favored the N_2O activation.

On the whole, on Co-MOR-73 pre-saturation with N_2O favored methane activation suggesting that O_{ads}^* arising from N_2O was necessary to activate CH_4; on Ni-MOR-80 pre-saturation with CH_4 favored N_2O reduction, suggesting that pre-reduction by CH_4 of Ni^{2+} to Ni^+ was necessary to activate N_2O; on Fe-MOR-64, where we detected two families of the Fe^{3+} dimers with different reducibility (UV–vis evidence), the first family, that was reduced to Fe^{2+} dimers during activation, behaved as Co^{2+} in Co-MOR, whereas the second family, that was reduced to Fe^{2+} dimers with CH_4, behaved as Ni^+ in Ni-MOR.

3.3.3. Surface species during N_2O reduction in the presence of O_2 detected by Operando FTIR

In all tmi-MOR *operando* FTIR spectra during the SCR_{N_2O} reaction at increasing temperature showed formaldehyde and type-II formate species (1590 cm^{-1}), as during CR_{N_2O}, whereas no methoxy species and type-I formates (1560 cm^{-1}) were detected (Fig. 11). In SCR_{N_2O} CH_xO_y intermediates formed in a lower amount than in CR_{N_2O}, suggesting their higher reactivity with O_2 than with N_2O. In Fe-MOR-64, little amount of carbonates at 1510 cm^{-1} were visible at low temperature, possibly due to formate oxidation on Fe-O-Fe species (Fig. 11b). On the other hand, since operando experiments under $CH_4 + O_2$ feed at increasing temperature showed no CH_xO_y bands in all tmi-MOR (spectra not shown), CH_xO_y intermediates in SCR_{N_2O} arose from oxidation of CH_4 by N_2O, as in CR_{N_2O}, while O_2 participated to the SCR reaction in a subsequent oxidative step.

On Co-MOR-73, to clarify oxidability of surface species, we added O_2 to the flow after surface pre-saturation with $CH_4 + N_2O$ feed at 623 K, following the evolution of the species as a function of time (Fig. 12). The intensity of the bands of the type-I formate and of methoxy decreased with time and progressively disappeared, whereas that of the bands of the type-II formate and of formaldehyde (1625 cm^{-1}) remained constant (see difference spectrum in Fig. 12). This result indicated a lower oxidability of the type-II formates with respect to type-I ones. We suggest that type-I formates were the reactive species yielding the final products of N_2O reduction, whereas type-II formates were more stable.

3.3.4. Reaction pathway and active site location for N_2O reduction by methane

For N_2O reduction, *operando* FTIR investigation indicated that on all catalysts the CH_xO_y intermediate formed by a surface reaction between N_2O and CH_4, because molecular O_2 was unable to activate CH_4. The active center O_{ads}^*, arising from N_2O activation, was able to activate methane, forming methoxy species with H-extraction. In the CR_{N_2O}, the methoxy species were subsequently oxidized step by step to formaldehyde and to formate species by other N_2O molecules up to final products (CO_2, H_2O, CO, H_2, according to a–d reactions), finally restoring the active tmi sites. In the SCR_{N_2O}, the oxidative steps of methoxy species were also performed by O_2. The catalytic activity combined with characterization results suggested that the active site (oxidation state, nuclearity and location) and the overall reaction pathways differed on each catalyst.

On Co-MOR-73 for CR_{N_2O}, as in N_2O decomposition, isolated Co^{2+} activated N_2O and yielded $Co^{3+}O^-$ intermediate, that oxidized CH_4 to methoxy. To have information on the active Co^{2+} location we investigated samples at different Co-content (from 23 to 89% of exchange) and correlated the activity with the Co site-population, that we previously evaluated by FTIR quantitative analysis of Co^{2+}-CO species [38,40]. By using this procedure, in previous papers on N_2O decomposition and on SCR_{N_2O} [37,38] we concluded that isolated Co^{2+}

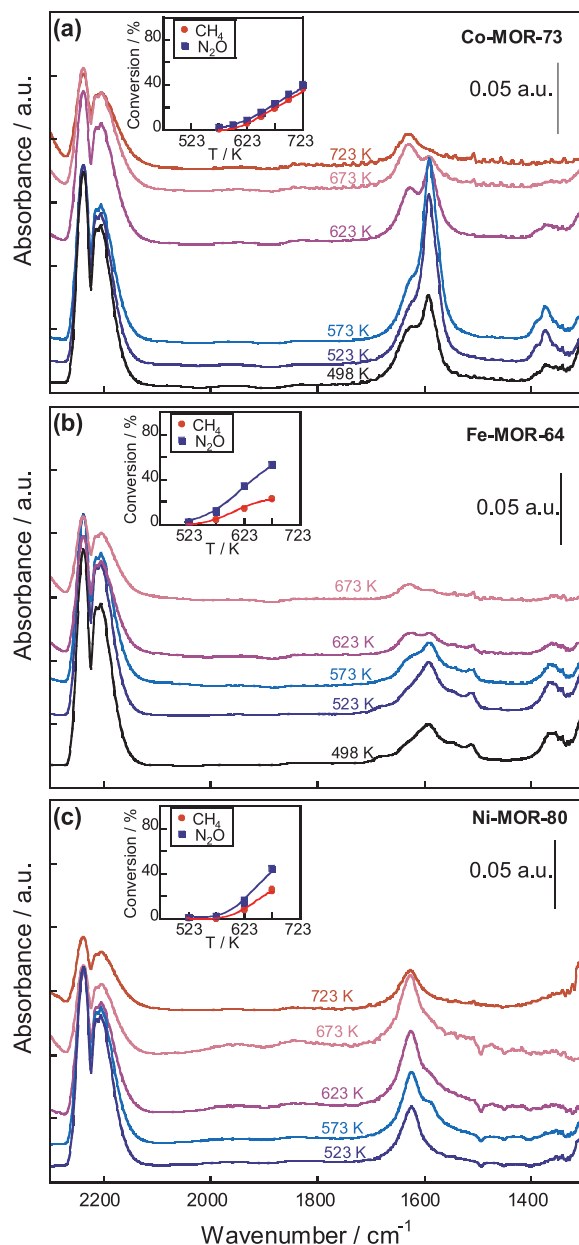**Fig. 11.** *Operando* FTIR spectra of surface species during SCR_{N_2O} reaction at increasing temperature on *standard activated* Co-MOR-73 (Section a), Fe-MOR-64 (Section b), and Ni-MOR-80 (Section c) catalysts. In the inset, the corresponding reactant conversions as a function of temperature. Reactant mixture: $[N_2O] = [CH_4] = 0.4\%$, $[O_2] = 2\%$ (total flow rate = 50 cm^3 STP/min, He as balance).

species located in both main channels and small channels were active for decomposition [37], whereas those in small channels were active for SCR_{N_2O} [38]. In the present paper, we found that the N_2O conversion for CR_{N_2O} increased markedly up to 23% exchange degree and remained at nearly the same level at higher Co-content (Fig. 13a), and that at a given temperature the rate of N_2O reduction increased with increasing Co-content as the population of the Co^{2+} in small channels, similarly to SCR_{N_2O} (Fig. 13b to be compared with Fig. 11c in ref. [38]). On the basis of (i) the rate dependence on site population (Fig. 13b), (ii) the parallel increase of the bands due to CH_xO_y species and to Al-OH in D sites (Fig. 10b), and (iii) the higher rate of CH_xO_y formation on a surface pre-saturated with N_2O (Fig. 10b), we suggest that the site active for CR_{N_2O} was possibly an isolated Co^{2+} in A site with a nearby Al-O^- c.u.s. in D site. Specifically, isolated Co^{2+} activated N_2O forming

in the temperature range of CR_{N_2O} and SCR_{N_2O} reactions the catalyst was nearly inactive for CH_4 combustion and that under $CH_4 + O_2$ feed *operando* FTIR detected no CH_xO_y species, in SCR_{N_2O} the addition of molecular oxygen did not trigger the CH_4 activation, and therefore O_2 participated to the subsequent oxidative steps of CH_xO_y intermediates. In agreement with the reaction stoichiometry ($CH_4 + N_2O + 3/2\,O_2 \rightarrow N_2 + CO_2 + 2H_2O$, see Section 3.3.1), in the first oxidative reaction step one isolated Co^{2+} activated one N_2O molecule; afterward the $Co^{3+}O^-$ reacted with one CH_4 molecule to form methoxy species, that subsequently was oxidized by O_2 to reactive formate intermediates (type-I). Therefore the same site was active for both SCR_{N_2O} and CR_{N_2O}, namely the isolated Co^{2+} in site A with a nearby Al-O^- c.u.s. in D site. Isolated Co^{2+} in E sites, although able to form $Co^{3+}O^-$, had negligible activity for N_2O reduction possibly because poisoned by the stable type-II formate.

On Ni-MOR-80, that yielded no N_2O activation, the formation of adsorbed carbonyl species under CH_4 feed at the CR_{N_2O} light-off temperature (*operando* FTIR evidence, Fig. 10c) suggested that CH_4 reacted with the oxygen of dimeric [Ni^{2+}-O-Ni^{2+}] species, yielding [Ni^+-(CO)-Ni^+]. The reactivity of Ni^{2+} dimers with CH_4 was similar to that found in Ni-MFI for (μ-oxo)dinickel species, that oxidized methane to methanol [60]. Under $CH_4 + N_2O$ feed the higher rate of CH_xO_y formation after preliminary CH_4 addition indicated that the Ni^+ dimers, arising from Ni^{2+} dimers reduction, yielded the N_2O activation and the formation of CH_xO_y species, subsequently oxidized up to final products.

On Fe-MOR-64, Fe^{3+} exchanged species, as Ni^{2+} in Ni-MOR, did not react with N_2O and a preliminary step of Fe^{3+} reduction by high temperature activation needed to yield active Fe^{2+} dimeric sites able to decompose N_2O. Under $CH_4 + N_2O$ feed at high temperature, the reducing CH_4 possibly formed the second type of Fe^{2+} dimers, that were detected by UV–vis DRS after CO reductive treatment. Similarly to that reported for the two types of Cu-O-Cu dimers stabilized in MOR [45], the different location of Fe^{2+} dimers in the framework could be the reason for their different reactivity. By reaction with N_2O, all the Fe^{2+} dimers yielded Fe^{3+}-$O^{(1+\delta)-}$—$Fe^{(2+\delta)+}$ intermediates that oxidized CH_4 to methoxy species. An analogous reaction pathway was proposed on Fe-BEA [29]. The O_{ads}^* species behaved similarly to the so-called α-oxygen, that was a labile oxygen species able to oxidize CH_4 to methanol on Fe-zeolites [48].

In Ni-MOR-80 and Fe-MOR-64, among the dimeric species located in the main channels or in the interconnecting side pockets of MOR, only those reduced to the proper oxidation state (Fe^{2+} and Ni^+ dimers) and with the two tmi sites at the proper distance were active sites favoring the bifunctional pathway for N_2O and CH_4 activation.

4. Conclusions

In tmi-exchanged mordenites (tmi = Co, Fe and Ni), *in situ* UV–vis DRS, *in situ* FTIR characterization and *operando* FTIR experiments combined with catalytic results give information on the tmi species working during N_2O abatement and on the reaction pathways.

For N_2O decomposition the activity order is Co-MOR > Fe-MOR in the absence of NO and Fe-MOR ≥ Co-MOR in the presence of NO, whereas Ni-MOR is always inactive. The decomposition occurs *via* cationic redox mechanism: active tmi sites are oxidized by N_2O, leaving on the surface activated atomic oxygen (O_{ads}^*), and are subsequently reduced by O_2 desorption. In Co-MOR all isolated Co^{2+} species in main and small channels yield $Co^{3+}O^-$ intermediates, that react with a second N_2O molecule yielding O_2 desorption *via* Eley-Rideal mechanism. In Fe-MOR, a preliminary high temperature treatment yields the release of the most labile bridged oxygen from Fe^{3+} dimers and the so formed [Fe^{2+}-□-Fe^{2+}] species react with N_2O yielding Fe^{3+}-$O^{(1+\delta)-}$—$Fe^{(2+\delta)+}$ intermediates. The quasi-oxidic character of oxygen species in this intermediate with respect to the oxyl character in $Co^{3+}O^-$ accounts for the lower activity and for the activity enhancement by NO addition to the feed of Fe-MOR with respect to Co-MOR. In
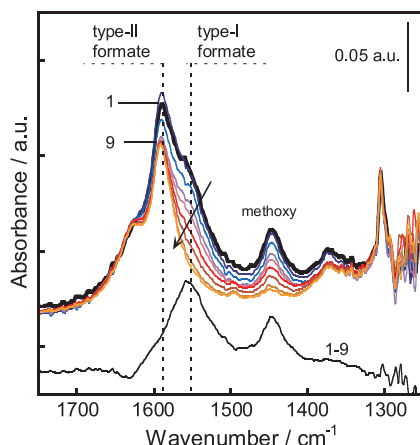

Fig. 12. *Operando* FTIR spectra of surface species on *standard activated* Co-MOR-73 catalyst after saturation under $N_2O + CH_4$ flow at 623 K (spectrum 1, bold line) and after subsequent addition to the feed of O_2 at increasing times (1, 3, 5, 8, 13, 17, 26 and 33 min, spectra from 2 to 9). The difference between spectrum 1 and spectrum 9 (1–9) is also reported. Reactant mixture: [N_2O] = [CH_4] = 0.4%, [O_2] = 2.0%, balance He (total flow = 50 cm³ STP/min).
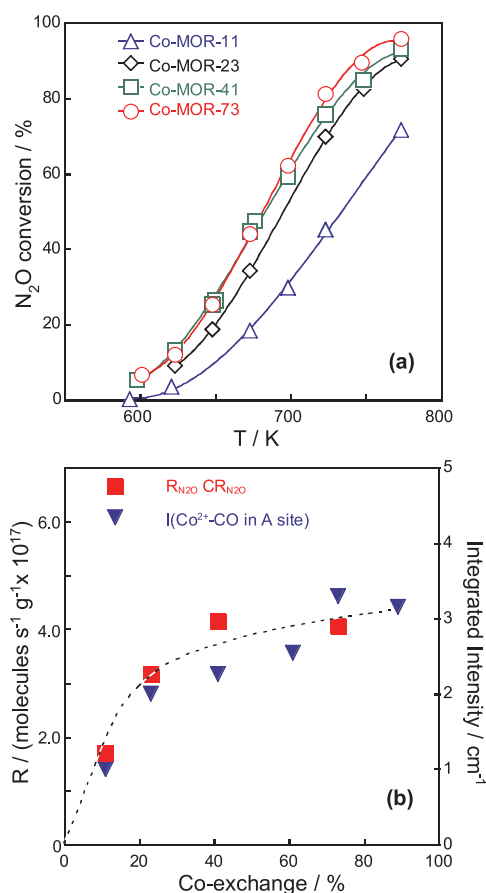

Fig. 13. CR_{N_2O} reaction on Co-MOR catalysts at increasing Co-content. Section a: percent N_2O conversion as a function of temperature, catalysts as indicated. Section b: correlation between rate of N_2O abatement in CR_{N_2O} reaction (R_{N_2O}/molecules s^{-1} g^{-1}) and integrated intensity (I/cm^{-1}) of $Co^{2+}-CO$ in A-sites, as a function of Co-exchange percent.

$Co^{3+}O^-$. Those in A sites, together with the Al-O^- c.u.s. in D site, formed CH_3O^- species with H-atom extraction from CH_4 on the nearby Al-O^-, namely *via* a bifunctional pathway. These methoxy species were subsequently oxidized up to the final products. Taking into account that

Ni-MOR, both isolated or dimeric Ni^{2+} species are unable to be oxidized by N_2O yielding O_{ads}^*.

For N_2O reduction with CH_4, in the absence or in the presence of O_2, the activity order is Fe-MOR > Ni-MOR > Co-MOR. The reduction requires the activation of N_2O and of CH_4. N_2O activation occurs on the tmi sites able to form the O_{ads}^* species. Subsequently, only the O_{ads}^* species having a nearby site at a proper distance are able to activate CH_4 *via* hydrogen extraction, yielding methoxy species, furtherly oxidized to formaldehyde and reactive formate species (type-I) by N_2O or O_2 molecules (*operando* FTIR evidence) up to final products. In Co-MOR, the bifunctional pathway occurs on isolated Co^{2+} in A sites with a nearby AlO^- in D sites. The formation of stable formate species (type-II) accounted for negligible N_2O reduction activity of the isolated Co^{2+} in E sites. In Ni-MOR, the presence of the CH_4 as reductant guarantees the formation of $[Ni^+\text{-}\square\text{-}Ni^+]$ dimers suitable for N_2O activation. In Fe-MOR, besides the first family of $[Fe^{2+}\text{-}\square\text{-}Fe^{2+}]$ due to the activation treatment, a second family of $[Fe^{2+}\text{-}\square\text{-}Fe^{2+}]$ forms in the presence of CH_4, both families able to activate N_2O. The Fe^{2+} and Ni^+ dimers, located in the main channels or in the interconnecting side pockets of MOR, having the two tmi sites at the proper distance favor the bifunctional pathway for N_2O and CH_4 activation.

We conclude that in Co-, Fe- and Ni-MOR the formation and the stability of O_{ads}^* surface species are key factors for N_2O abatement. Both the factors were affected by the mobility of the tmi electrons, that depends on the tmi oxidation state, nuclearity and location in MOR framework.

Acknowledgements

References

[1] WMO, WMO Greenhouse Gas Bull. 7 (2011) 1–4.
[2] WMO, WMO Greenhouse Gas Bull. 12 (2016) 1–8.
[3] M. Konsolakis, ACS Catal. 5 (2015) 6397–6421.
[4] J. Pérez-Ramírez, Appl. Catal. B 70 (2007) 31–35.
[5] J. Pérez-Ramírez, F. Kapteijn, K. Schöffel, J.A. Moulijn, Appl. Catal. B 44 (2003) 117–151.
[6] Brochures of EnviNOx, are available at http://www.uhde.biz.
[7] F. Kapteijn, J. Rodriguez-Mirasol, J.A. Moulijn, Appl. Catal. B 9 (1996) 25–64.
[8] Y. Li, J.N. Armor, Appl. Catal. B 1 (1992) L21–L29.
[9] F. Kapteijn, G. Marban, J. Rodriguez-Mirasol, J.A. Moulijn, J. Catal. 167 (1997) 256–265.
[10] B.R. Wood, J.A. Reimer, A.T. Bell, J. Catal. 209 (2002) 151–158.
[11] D. Pietrogiacomi, M.C. Campa, M. Occhiuzzi, Catal. Today 227 (2014) 116–122.
[12] K. Jíša, J. Nováková, M. Schwarze, A. Vondrová, S. Sklenák, Z. Sobalik, J. Catal. 262 (2009) 27–34.
[13] C. Sang, C.R.F. Lund, Catal. Lett. 73 (2001) 73–77.
[14] P. Sazama, B. Wichterlová, E. Tábor, P. Šťastný, N.K. Sathu, Z. Sobalík, J. Dědeček, Š. Sklenák, P. Klein, A. Vondrová, J. Catal. 312 (2014) 123–138.
[15] El-M. El-Malki, R.A. van Santen, W.M.H. Sachtler, J. Catal. 196 (2000) 212–223.
[16] A. Guzmán-Vargas, G. Delahay, B. Coq, Appl. Catal. B 42 (2003) 369–379.
[17] T. Nobukawa, M. Yoshida, S. Kameoka, S.-I. Ito, K. Tomishige, K. Kunimori, Catal. Today 93–95 (2004) 791–796.
[18] M. Kögel, R. Mönnig, W. Schwieger, A. Tissler, T. Turek, J. Catal. 182 (1999) 470–478.
[19] S. Kameoka, T. Nobukawa, S. Tanaka, S. Ito, K. Tomishige, K. Kunimori, Phys. Chem. Chem. Phys. 5 (2003) 3328–3333.
[20] M.N. Debbagh, C. Salinas-Martínez de Lecea, J. Pérez-Ramírez, Appl. Catal. B 70 (2007) 335–341.
[21] G. Delahay, M. Mauvezin, A. Guzmán-Vargas, B. Coq, Catal. Commun. 3 (2002) 385–389.
[22] S. Kameoka, K. Kita, S. Tanaka, T. Nobukawa, S. Ito, K. Tomishige, T. Miyadera, K. Kunimori, Catal. Lett. 79 (2002) 63–67.
[23] T. Chaki, M. Arai, T. Ebina, M. Shimokawabe, J. Mol. Catal. A: Chem. 227 (2005) 187–196.
[24] M.A.G. Hevia, J. Pérez-Ramírez, Environ. Sci. Technol. 42 (2008) 8896–8900.
[25] G. Moretti, G. Fierro, G. Ferraris, G.B. Andreozzi, V. Naticchioni, J. Catal. 318 (2014) 1–13.
[26] J. Pérez-Ramírez, G. Mul, F. Kapteijn, J.A. Moulijn, Kinet. Catal. 44 (5) (2003) 639–647.
[27] J. Pérez-Ramírez, M.S. Kumar, A. Brückner, J. Catal. 223 (2004) 13–27.
[28] T. Nobukawa, M. Yoshida, K. Okumura, K. Tomishige, K. Kunimori, J. Catal. 229 (2005) 374–388.
[29] T. Nobukawa, M. Yoshida, S. Kameoka, S. Ito, K. Tomishige, K. Kunimori, J. Phys. Chem. B 108 (2004) 4071–4079.
[30] J. Dědeček, Z. Sobalík, B. Wichterlová, Catal. Rev.: Sci. Eng. 54 (2012) 135–223.
[31] M. Rivallan, G. Ricchiardi, S. Bordiga, A. Zecchina, J. Catal. 264 (2009) 104–116.
[32] A.L. Yakovlev, G.M. Zhidomirov, R.A. van Santen, J. Phys. Chem. B 105 (2001) 12297–12302.
[33] K.A. Dubkov, N.S. Ovanesyan, A.A. Shteinman, E.V. Starokon, G.I. Panov, J. Catal. 207 (2002) 341–352.
[34] Z. Sobalík, J. Novakova, J. Dědeček, N.K. Sathu, E. Tábor, P. Sazama, P. Šťastný, B. Wichterlová, Microporous Mesoporous Mater. 146 (2011) 172–183.
[35] X. Zhang, Q. Shen, C. He, C. Ma, J. Cheng, Z. Liu, Z. Hao, Catal. Sci. Technol. 2 (2012) 1249–1258.
[36] P.J. Smeets, Q. Meng, S. Corthals, H. Leeman, R.A. Schoonheydt, Appl. Catal. B 84 (2008) 505–513.
[37] M.C. Campa, V. Indovina, D. Pietrogiacomi, Appl. Catal. B 91 (2009) 347–354.
[38] M.C. Campa, D. Pietrogiacomi, M. Occhiuzzi, Appl. Catal. B 168–169 (2015) 293–302.
[39] V. Indovina, M.C. Campa, D. Pietrogiacomi, J. Phys. Chem. C 112 (2008) 5093–5101.
[40] M.C. Campa, I. Luisetto, D. Pietrogiacomi, V. Indovina, Appl. Catal. B 46 (2003) 511–522.
[41] O. Marie, P. Massiani, F. Thibault-Starzyk, J. Phys. Chem. B 108 (2004) 5073–5081.
[42] A. Martucci, G. Cruciani, A. Alberti, C. Ritter, P. Ciambelli, M. Rapacciuolo, Microporous Mesoporous Mater. 35–36 (2000) 405–412.
[43] W.J. Mortier, Compilation of extraframework sites in zeolites, Zeolites (1982).
[44] J. Dědeček, B. Wichterlová, J. Phys. Chem. B 103 (1999) 1462–1476.
[45] P. Vanelderen, B.E.R. Snyder, M.-L. Tsai, R.G. Hadt, J. Vancauwenbergh, O. Coussens, R.A. Schoonheydt, B.F. Sels, E.I. Solomon, J. Am. Chem. Soc. 137 (2015) 6383–6392.
[46] D.W. Barnum, Inorg. Chem. 22 (1983) 2297–2305.
[47] L. Čapek, V. Kreibich, J. Dědeček, T. Grygar, B. Wichterlová, Z. Sobalík, J.A. Martens, R. Brosius, V. Tokarová, Microporous Mesoporous Mater. 80 (2005) 279–289.
[48] E.V. Starokon, K.A. Dubkov, L.V. Pirutko, G.I. Panov, Top. Catal. 23 (2003) 137–143.
[49] P. Sazama, N.K. Sathu, E. Tábor, B. Wichterlová, Š. Sklenák, Z. Sobalík, J. Catal. 299 (2013) 188–203.
[50] A. Zecchina, M. Rivallan, G. Berlier, C. Lamberti, G. Ricchiardi, Phys. Chem. Chem. Phys. 9 (2007) 3483–3499.
[51] G.D. Pirngruber, P.K. Roy, R. Prins, J. Catal. 246 (2007) 147–157.
[52] P.J. Smeets, J.S. Woertink, B.F. Sels, E.I. Solomon, R.A. Schoonheydt, Inorg. Chem. 49 (8) (2010) 3573–3583.
[53] M. Occhiuzzi, G. Fierro, G. Ferraris, G. Moretti, Chem. Mater. 24 (2012) 2022–2031.
[54] A.B.P. Lever, Inorganic Electron Spectroscopy, 2nd ed., Elsevier, Amsterdam, 1984, p. 468.
[55] J. Pérez-Ramírez, F. Kapteijn, G. Mul, J.A. Moulijn, J. Catal. 208 (2002) 211–223.
[56] H. Xia, K. Sun, Z. Liu, Z. Feng, P. Ying, C. Li, J. Catal. 270 (2010) 103–109.
[57] V. Blasin-Aubeˊ, O. Marie, J. Saussey, A. Plesniar, M. Daturi, N. Nguyen, C. Hamon, M. Mihaylov, E. Ivanova, K. Hadjiivanov, J. Phys. Chem. C 113 (2009) 8387–8393.
[58] G. Busca, A.S. Elmi, P. Forzatti, J. Phys. Chem. 91 (1987) 5263–5269.
[59] C.-T. Wang, R.J. Willey, J. Catal. 202 (2001) 211–219.
[60] J. Shan, J. Huang, W. Nguyen, Y. Yu, S. Zhang, Y. Li, A.I. Frenkel, F.F. Tao, Langmuir 30 (2014) 8558–8569.